IEEE Access
Multidisciplinary ⋮ Rapid Review ⋮ Open Access Journal

Received 28 June 2023, accepted 5 August 2023, date of publication 17 August 2023, date of current version 28 August 2023.

Digital Object Identifier 10.1109/ACCESS.2023.3305919

RESEARCH ARTICLE

A New Algorithm for Multi-Area Power Flow

ROBERTO BENATO, (Senior Member, IEEE), AND GIOVANNI GARDAN, (Member, IEEE)
Department of Industrial Engineering, University of Padova, 35131 Padua, Italy
Corresponding author: Roberto Benato (roberto.benato@unipd.it)

ABSTRACT In this paper, a new algorithm computing the multi-area power flow problem is presented. This algorithm is suitable for AC synchronous areas operating in steady-state conditions and interconnected by means of AC tie-lines. In particular, a new iterative composition/decomposition matrix procedure is adopted. For each area, the classical PV, PQ, and slack bus constraints are defined, allowing the computation of the power flow of each area independently. This independency of the power flow solution of each area allows exploiting the parallel computation technique. The overall power flow is then computed by putting together all the solutions of each area iteratively, by means of the tie-line (*i.e.,* the lines interconnecting the areas) admittance matrix. The present multi-area method is novel and completely general and once the power flow solution of each area is separately achieved by any power flow solver (e.g., Newton-Raphson and derived, PFPD, or other), it makes suitable use of both a Thevenin's theorem generalization and a novel tie-line admittance matrix. In this direction, the method is not a new power flow algorithm but a new multi-area algorithm, which starts from the solutions of the power flow of each area, each considered with its own slack-bus. Applications of the algorithm to standard test cases are presented. Eventually, to test the validity of the method, numerical comparisons with the commercial software DIgSILENT PowerFactory are performed.

INDEX TERMS AC/DC transmission networks, distributed slack bus, multi-area power flow, multi-area power systems, parallel computing.

NOMENCLATURE

Symbol	Quantity
A. Acronyms	
PFPD	Power Flow of the University of Padova
PFPD-X	Algorithm of the University of Padova for multi-area power flow
ENTSO-E	European association for the cooperation of TSOs for electricity
RES	Renewable Energy Sources
HVAC	High Voltage Alternate Current
HVDC	High Voltage Direct Current
PCC	Point of Common Coupling
PV	Active power (P) generation and voltage magnitude (V) constrained in a bus
PQ	Active (P) and reactive (Q) power constrained in a bus
DGS	Commercial software DIgSILENT PowerFactory
TSO	Transmission System Operator
OPF	Optimal Power Flow
PFC	Power Flow Controller
PST	Phase Shift Transformer
ITER	Number of iterations of PFPD-X

B. Sets and Indices

A, B, C	Areas A, B, C
S_A, S_B, S_C	Cross-border sections of areas A, B, C
k	k^{th} iteration of PFPD-X
sched	Scheduled quantity
n	Number of areas of the overall system

C. Variables and Parameters

$\underline{u}_{a,r,A}$	Slack bus voltage phasor of area A
$\vartheta_{ar,A}$	Slack bus voltage angle of area A
$\underline{\boldsymbol{Y}}_{\boldsymbol{tie}}$	Admittance matrix of the AC lie-lines
$\underline{\boldsymbol{Z}}_{\boldsymbol{Aeq}}$	Equivalent impedance matrix of area A as seen from the cross-border section S_A
$\underline{\boldsymbol{e}}_{\boldsymbol{0A}}, \underline{\boldsymbol{e}}_{\boldsymbol{0B}}\ \underline{\boldsymbol{e}}_{\boldsymbol{0C}}$	Voltage phasors at each area without interconnections

The associate editor coordinating the review of this manuscript and approving it for publication was Tariq Masood.

$\underline{\boldsymbol{e}}$	Vector of the voltage phasors of all the cross-border sections
$\underline{\boldsymbol{i}}$	Vector of the current entering into al the cross-border sections
$\underline{\boldsymbol{Z}}_{\boldsymbol{eq}}$	Equivalent impedance matrix of all the areas of the overall system
$\aleph$	Iterative matrix linking the voltage phasor vectors without interconnections and with interconnections
$y'_{\mathrm{SAI}}, y'_{\mathrm{SAII}}$	Self-admittances at cross-section A modelling the first (I) and second (II) tie-lines of area A
$\underline{\boldsymbol{Y}}_{\boldsymbol{inter}}$	Admittance matrix storing the self-admittances at cross-section A
tol	Tolerance of PFPD-X

I. INTRODUCTION

A. MOTIVATION

In 2022, Benato presented the ''open'' matrix power flow algorithm PFPD, based on the all-inclusive complex admittance matrix also including the slack bus [1]. The good results of [1] encouraged the authors to extend PFPD to this new matrix algorithm for multi-area applications. The authors immediately wish to stress the concept of ''open''. The term ''open'' refers to the philosophy of sharing algorithm formulations in detail, encouraging researchers to critically self-implement the procedure and, in case, to debate with the scientific community about the procedures and their use (unlike closed software, in which it cannot be seen what is inside).

We have a multi-area power system whenever different areas are interconnected among them in a unique network. This is a reality especially for large bulk power systems (*e.g.* the European ENTSO-E transmission network [2], [3] and the North American one [4], [5]) and in the next future, the growing interconnection process could bring to a unique global interconnected power system [6], [7]. This would allow Renewable Energy Sources (RES) to massively penetrate the global power system [8]. The first step in designing, planning, and analyzing the multi-area power systems is the power flow analysis, which studies the steady-state operation of any network.

According to authors, the motivation why the multi-area networks are challenging to assess are two.

Firstly, being large interconnected system, they can be characterized by a huge number of elements (+10000 buses to +100000 buses), therefore a computational burden may arise even for a power flow study. Moreover, studies where power flow in series must be run (like Monte Carlo analyses in probabilistic power flow or Continuation power flows) could be very expensive from a computational point of view.

Secondly, a multi-area power flows should be studied by means of a multi-area approach, and not with the classical power flow. Physically, in fact, whenever the classical power flow formulation is considered, a unique slack generator is defined in order to fix the power balance between generation and absorption (including power losses of each area). However, it would be physically unrealistic that a unique slack generator fixes the power balance of the overall network. It would make sense if each area had its own slack generator fixing the balance of active and reactive power (including power losses).

The authors are keen to stress the difference between the terms ''swing'' and ''slack'' when they refer to the generator. The term ''swing'' refers to the angle reference imposed by a generator voltage phasor (typically set to zero). The term ''slack'' refers to the generator adjusting the power balance between the generation and absorption (so giving all the network power losses) in the power flow problem.

B. LITERARY REVIEW

The above-mentioned research topics recall the Kron's ideas, introduced in the 50s, of *diakoptics* [9]. The idea of diakoptics is to tear large systems into smaller ones, to compute their solutions, and put them together to gain the overall solution [9], [10], [11], [12], [13]. Such studies flourished from the 70s and were justified by the search for advantageous methods in terms of computer-core-storage requirements. The main mathematical piecewise techniques are firstly exposed in [9]; in [10] power flow formulations based on graph-cutting techniques with departures from the usual slack bus treatment are taken; in [11] cut lines are considered as injecting-current elements which must be compensated consistently inside the equations of each area; while in [12] and [13] algebraic graph theory manipulations are introduced to modify the topological equations to be used for the power flow formulation.

All the above methods are long abandoned, since they are considered difficult to understand, and since the progress of digital computers in power system computations made these piecewise algorithms unnecessary.

The bulk power systems are becoming AC/DC ones, and two possible tie-line technologies can interconnect multi-area power systems: HVDC and HVAC links. From a multi-area point of view, these two types of links have the following characteristics:

1. HVDC tie-lines: in [14] HVDC links can be eliminated by considering only PV/PQ constraints in the PCC (Points of Common Coupling). This is possible since the typical steady state HVDC converter controls [14] decouple linked systems. Therefore, power flow for each area can be computed independently, by considering different slack buses for each area.
2. HVAC tie-lines: in a synchronous multi-area network, the overall system cannot be decoupled since the sub-systems influence each other. Therefore, only one swing generator (not slack!) should be defined to have a voltage phasor reference for the overall system.

It is well-known, however, that in classical power flow problems, slack generator is only a mathematical artifice [15].

In fact, from a physical standpoint, the slack generator gives all the system power losses. Thus, the active/reactive power balance due to a unique generator can jeopardize the voltage evaluation especially near the slack generator. Such misleading evaluations are heavier for large systems. In technical literature participant factors for a distributed slack approach were developed [15], [16]. However, such studies are more suitable for economic dispatch problems. It would be appropriate, for a classical multi-area approach, to have a slack generator for each area [17], so giving a solution more adherent to physical reality.

C. CONTRIBUTION

An iterative procedure solving separately and connecting together the power flow solutions for each area of any multi-area system is presented.

To consider the impact of the interconnections, new PQ-constraints at the borders of each area are computed iteratively. This idea arises from the fact that at the border of each area there is an injection/absorption of active (P) and reactive (Q) power. Therefore, the main function of the algorithm is to define iteratively such constraints by means of the iterative matrix technique presented. Each power flow is computed after defining its own slack generator.

It is advantageous to use the present algorithm with the power flow open algorithm PFPD, due to its good computational performances [1]. However, the multi-area procedure is totally general, and the power flow of each area can be achieved separately with any other power flow method (e.g., Newton-Raphson and derived).

Another contribution consists in modifying the angle phasor of some control-area swing generators to make a scheduled amount of active power flow in specific lines (''the swing-correction procedure''). This task is considered as a sub-application of the basic method presented in this paper that allows modifying some active power flowing in some (n-1 as it will be explained) lines interconnecting the system. This can be an alternative method in case Optimal Power Flow fails.

The algorithm is tested on a 3-area reference network. A method to compare the results with the commercial software DIgSILENT PowerFactory (DGS) is described. Such comparisons with DGS validate the algorithm. Numerical simulations are widely discussed by showing both results and performances of the algorithm.

The development of the algorithm has been not intended as a substitution of other multi-area methods, but rather as an alternative approach to the steady-state operation of such systems. In fact, authors believe that the more the methods model a problem, the better the understanding of the matter (i.e. about multi-area power systems analysis).

II. FORMULATION OF PFPD-X

This novel multi-area power flow algorithm (in the following indicated as PFPD-X) is presented with reference to Fig. 1. It deals with a 3-area power system, where each area (A, B, C) is connected by means of a given set of tie-lines. It is worth noting in Fig. 1 that each area presents its slack generator (it is represented as a quasi-ideal current source according to PFPD [1]). The voltage phasor imposed by the current sources namely $\underline{u}_{ar,A}$, $\underline{u}_{ar,B}$, $\underline{u}_{ar,C}$ must be kept constant and in phase (*e.g.*, $\vartheta_{ar,A}=\vartheta_{ar,B}=\vartheta_{ar,C}=0°$) during the multi-area solution procedure. This choice seems to be significant for real multi-area power systems, where each Transmission System Operator (TSO) solves its own power flow with a chosen slack-bus, satisfying its own active/reactive power balances (including losses).

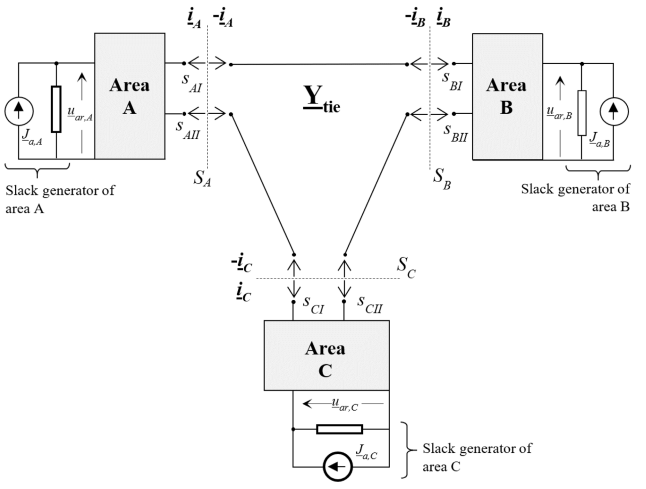

FIGURE 1. Subdivision of the entire grid into three areas A, B, and C with tie-lines.

The tie-lines can be represented by means of their nodal admittance matrix $\underline{\boldsymbol{Y}}_{\boldsymbol{tie}}$.

Firstly, the power flow solution of each area is computed separately from the entire network: the voltage phasors of each area become known quantities. The voltages at the cross-border sections S_A, S_B, S_C considered without the interconnection tie-lines are indicated as $\underline{\boldsymbol{e}}_{\boldsymbol{0A}}, \underline{\boldsymbol{e}}_{\boldsymbol{0B}}\ \underline{\boldsymbol{e}}_{\boldsymbol{0C}}$.

When the tie-lines are considered, they cause current injections into the three areas A, B and C at the cross-borders S_A, S_B, S_C yielding the tensor relation (1):

$$\begin{bmatrix} \underline{\boldsymbol{e}}_A \\ \underline{\boldsymbol{e}}_B \\ \underline{\boldsymbol{e}}_C \end{bmatrix} = \begin{bmatrix} \underline{\boldsymbol{e}}_{0A} \\ \underline{\boldsymbol{e}}_{0B} \\ \underline{\boldsymbol{e}}_{0C} \end{bmatrix} + \begin{bmatrix} \underline{\boldsymbol{Z}}_{Aeq} & \boldsymbol{0} & \boldsymbol{0} \\ \boldsymbol{0} & \underline{\boldsymbol{Z}}_{Beq} & \boldsymbol{0} \\ \boldsymbol{0} & \boldsymbol{0} & \underline{\boldsymbol{Z}}_{Ceq} \end{bmatrix} \cdot \begin{bmatrix} \underline{\boldsymbol{i}}_A \\ \underline{\boldsymbol{i}}_B \\ \underline{\boldsymbol{i}}_C \end{bmatrix} \tag{1}$$

where $\underline{\boldsymbol{Z}}_{\boldsymbol{Aeq}}, \underline{\boldsymbol{Z}}_{\boldsymbol{Beq}}, \underline{\boldsymbol{Z}}_{\boldsymbol{Ceq}}$ are the impedance matrices as seen from the cross-borders sections S_A, S_B, S_C respectively and $\underline{\boldsymbol{i}}_{\boldsymbol{A}}$, $\underline{\boldsymbol{i}}_{\boldsymbol{B}}$, $\underline{\boldsymbol{i}}_{\boldsymbol{C}}$ are the current vectors shown in Fig. 1. For the computation of $\underline{\boldsymbol{Z}}_{\boldsymbol{Aeq}}, \underline{\boldsymbol{Z}}_{\boldsymbol{Beq}}, \underline{\boldsymbol{Z}}_{\boldsymbol{Ceq}}$ see Sect. III.

Eq. (1) can be written in compact form as in the following:

$$\underline{\boldsymbol{e}} = \underline{\boldsymbol{e}}_{\boldsymbol{0}} + \underline{\boldsymbol{Z}}_{\boldsymbol{eq}}\, \underline{\boldsymbol{i}}$$

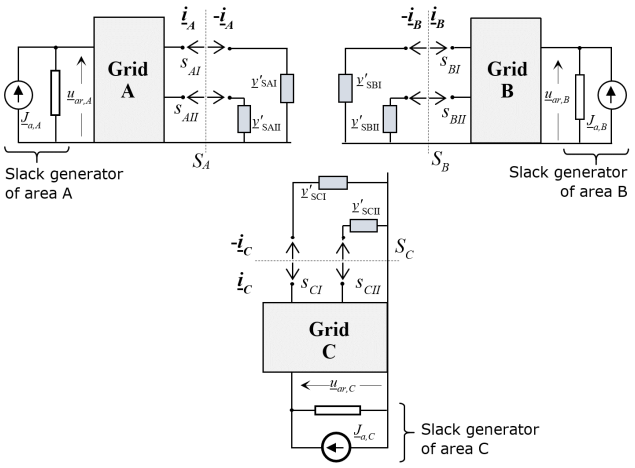

FIGURE 2. Modelling of the tie-lines connections by means of self-admittances as seen from each area.

The currents entering in each area can be computed by means of $\underline{\boldsymbol{Y}}_{tie}$:

$$\begin{bmatrix} \underline{i}_A \\ \underline{i}_B \\ \underline{i}_C \end{bmatrix} = - \underline{\boldsymbol{Y}}_{tie} \begin{bmatrix} \underline{e}_A \\ \underline{e}_B \\ \underline{e}_C \end{bmatrix} \tag{2}$$

which can be written in compact form as it follows:

$$\underline{i} = -\underline{\boldsymbol{Y}}_{tie}\, \underline{e}$$

By combining (1) and (2), it yields:

$$\underline{e} = \underline{e}_0 - \underline{\boldsymbol{Z}}_{eq}\, \underline{\boldsymbol{Y}}_{tie}\, \underline{e} \tag{3}$$

from which it is possible to derive (4) by simple matrix algebra:

$$\underline{e} = [\boldsymbol{I} + \underline{\boldsymbol{Z}}_{eq}\, \underline{\boldsymbol{Y}}_{tie}]^{-1}\, \underline{e}_0 \tag{4}$$

By defining the matrix $\underline{\aleph} = \boldsymbol{I} + \underline{\boldsymbol{Z}}_{eq}\, \underline{\boldsymbol{Y}}_{tie}$, (4) can be written as:

$$\underline{e} = \underline{\aleph}^{-1} \cdot \underline{e}_0 \tag{5}$$

and (2) can be written as (6):

$$\underline{i} = -\underline{\boldsymbol{Y}}_{tie} \aleph^{-1}\, \underline{e}_0 \tag{6}$$

By dividing all the cross-border currents (6) by the cross-border voltages (5), the cross-border self-admittances $\underline{y}'_{\mathrm{SAI}}$, $\underline{y}'_{\mathrm{SAII}}$, $\underline{y}'_{\mathrm{SBI}}$, $\underline{y}'_{\mathrm{SBII}}$, $\underline{y}'_{\mathrm{SCI}}$, $\underline{y}'_{\mathrm{SCII}}$ can be computed (see Fig. 2) at all cross-border nodes. As it can be seen in Sect. II. A, it is useful to store such admittances in the diagonal of the matrix $\underline{\boldsymbol{Y}}_{inter}$:

$$\underline{\boldsymbol{Y}}_{inter} = \mathrm{diag}(\underline{\boldsymbol{i}}./\underline{\boldsymbol{e}}) \tag{7}$$

where./ represent the element by element vector division.

Such self-admittances give a first initial guess of the effects of the interconnections as seen from each area. Eq. (5), in fact, gives an approximation of the cross-border voltages of the multi-area power system. This approximation is due to the block diagonal structure of (1): the voltage inter-dependence between the different areas is not represented, since it cannot be known *a priori*, but depends on the overall power flow solution.

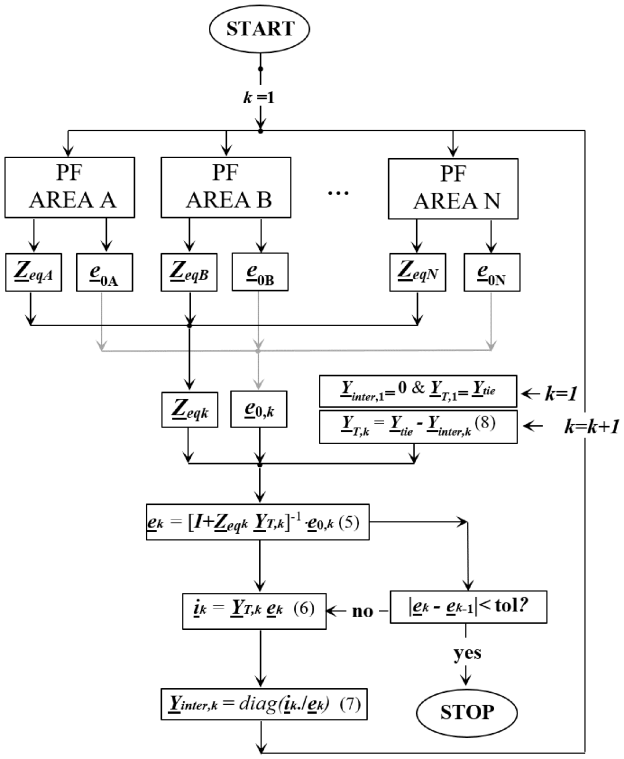

FIGURE 3. PFPD-X flow chart pattern for each iteration k.

Eq. (5) and (6) must be iterated to adjust the cross-border admittances representing the tie-lines as seen from each area.

A. PFPD-X: THE BASIC PROCEDURE

Fig. 3 summarizes the iterative procedure to compute the cross-border admittances equivalent to the tie-lines.

First, a power flow solution for each area (PF AREA A, PF AREA B, PF AREA C) is computed. For the sake of CPU time performance, these power flows can be computed in parallel. In the first cycle, the power flows are computed by preliminarly considering the areas without equivalent cross-border admittances, *i.e.*,

$$\underline{\boldsymbol{Y}}_{inter,1} = 0$$

From the power flow solutions of all the areas, it is possible to compute the impedance matrices ($\underline{\boldsymbol{Z}}_{A,1}$;$\underline{\boldsymbol{Z}}_{B,1}$;$\underline{\boldsymbol{Z}}_{C,1}$) and the no-load voltages ($\underline{\boldsymbol{e}}_{0A,1}$;$\underline{\boldsymbol{e}}_{0B,1}$;$\underline{\boldsymbol{e}}_{0C,1}$) as seen from the cross-borders sections S_A, S_B, S_C respectively.

As highlighted in Sect. III, the impedance matrices ($\underline{\boldsymbol{Z}}_{A,k}$;$\underline{\boldsymbol{Z}}_{B,k}$;$\underline{\boldsymbol{Z}}_{C,k}$) change with each iteration, since they depend on the k-th power flow solution. Therefore, (5), (6), and (7) compute the cross-border equivalent admittances to be stored in the diagonal admittance matrix $\underline{\boldsymbol{Y}}_{inter,2}$. Such

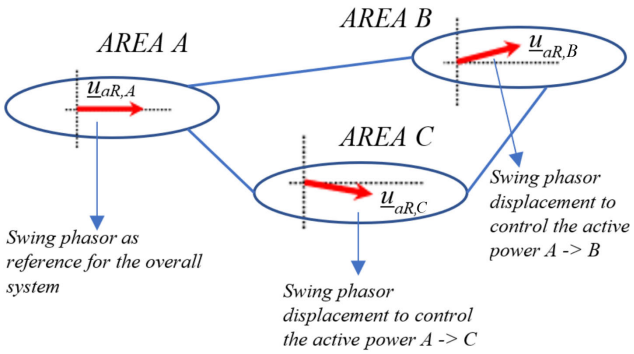

FIGURE 4. Example of swing angle correction in a 3-area system to the active power flowing in the tie-lines A->B and A->C.

admittances absorbing/injecting complex power are the new PQ constraints to be used in the next step (k=2) of the power flow computations. By considering the different areas as interconnected, it is necessary to define a new interconnection admittance matrix $\underline{\boldsymbol{Y}}_{\boldsymbol{T,2}} = \underline{\boldsymbol{Y}}_{\boldsymbol{tie}} - \underline{\boldsymbol{Y}}_{\boldsymbol{inter,1}}$:

$$\underline{\boldsymbol{Y}}_{\boldsymbol{T,k=2}} = \underline{\boldsymbol{Y}}_{\boldsymbol{tie}} - \begin{bmatrix} \underline{y}'_{\mathrm{SAI},k=1} & 0 & 0 \\ 0 & \cdots & 0 \\ 0 & 0 & \underline{y}'_{\mathrm{SCII},k=1} \end{bmatrix}$$

which can be generalized as it follows:

$$\underline{\boldsymbol{Y}}_{\boldsymbol{T,k}} = \underline{\boldsymbol{Y}}_{\boldsymbol{tie}} - \underline{\boldsymbol{Y}}_{\boldsymbol{inter,k}} \tag{8}$$

Therefore, (5), (6), and (7) can be exploited in order to compute the cross-border equivalent admittances $\underline{y}'_{\mathrm{SAI},k=2}$, $\underline{y}'_{\mathrm{SAII},k=2}$, $\underline{y}'_{\mathrm{SBI},k=2}$, $\underline{y}'_{\mathrm{SBII},k=2}$, $\underline{y}'_{\mathrm{SCI},k=2}$, $\underline{y}'_{\mathrm{SCII},k=2}$ to store in the diagonal admittance matrix $\boldsymbol{y}_{\boldsymbol{inter,2}}$. This pattern is repeated iteratively. The convergence is reached when the differences between all the cross-border voltage magnitudes of two consecutive cycles are lower than a given tolerance (tol.) *i.e.*,

$$|\underline{\boldsymbol{e}}_{\boldsymbol{k}} - \underline{\boldsymbol{e}}_{\boldsymbol{k-1}}| < \mathbf{tol}$$

As above stated, the procedure presented for "only" three areas is completely general and the complete iterative procedure is shown in Fig. 3.

B. PFPD-X: THE SWING-CORRECTION PROCEDURE

The solution of PFPD-X must be interpreted as it follows: it is the set of the power flow voltages that tie the areas together in a unique coherent power flow solution.

In the following, considerations on the possibility to exploit PFPD-X to control the active power flowing in some tie-lines is exploited.

1) COMPLEX POWER FLOWING IN AN AC TIE-LINE

The complex power flowing in a tie-line connecting two different areas can be easily computed with (9) [18]:

$$\underline{s}_s = -\frac{e_s e_r}{B} e^{j(\beta+\vartheta)} + \frac{e_r^2 D}{B} e^{j(\beta+\vartheta)}, \tag{9}$$

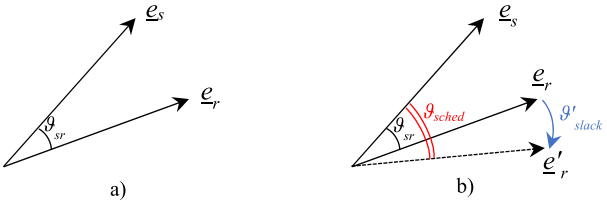

FIGURE 5. Phase angle shifts in a tie-line connecting two areas a) before the slack bus angle correction, and b) after the slack bus angle correction.

where e_a, e_p are the phase-to-ground voltage magnitudes of the sending and receiving areas; B (and β), D (and ϑ) are the magnitude (and the corresponding arguments) extracted from the hybrid ABCD matrix of the tie-line line.

2) ACTIVE POWER FLOW ADJUSTMENTS IN AC TIE-LINES

If the active power flowing on some tie-lines coming from (9) are not satisfying, it is possible to improve the active power level flowing in $n-1$ AC tie-lines, by acting on the swing generator angles of *n-1* areas.

However, a limitation of this fact is that only the flows of $n-1$ tie-lines can be controlled. By considering n areas, in fact, one swing generator must be set to zero to have a reference for the overall system. Fig. 4 shows an example on a three-area power system: the slack generator of area 1 is the angle reference of the buses of all the system, but the swing generator of areas 2 and 3 can be changed independently in order to impact on the transit of power on the two lines 1-2 and 1-3.

The limitation of that method is the possibility to control a limited number of AC tie-lines ($n-1$, *i.e.*, two lines in the case of Fig. 4), so the method is suitable when some adjustments (maximum $n-1$) must be done. Alternative methods like the OPF, in case they converge, can be exploited in order to control a bigger number of lines.

It is known, in fact, that the active power, flowing in a predominantly inductive link, is roughly related to the phasor displacement between the sending (s) and the receiving (r) ends:

$$P_{s\to r} \Rightarrow \vartheta_s - \vartheta_r$$

A power flow where the swing generator angle is shifted from a certain quantity (typically set to zero by convention), causes an angle displacement of all the voltage phasor of the same quantity. For instance, by considering Fig. 1, a desired active power flowing between area A and B can be obtained by considering swing bus angle $\vartheta_{a,A}$=0, and the swing bus angle $\vartheta_{b,B}$ set to the value allowing the flow of a certain quantity of active power in the considered tie-line.

These angle changes can be iteratively set inside PFPD-X, and the power flow solutions of the chosen areas change. In particular, new active power values from the slack generators are found; from the power conservation principle point of view, they are the active power that allow flowing a certain amount of active power in the chosen tie-line.

This swing-correction version of PFPD-X can be summarized with the following steps:

1. Considering a specific tie-line, during the k-th iterative cycle of the procedure shown in Fig. 3, the shift angle ($\vartheta_{sr} = \vartheta_s$-$\vartheta_r$) between the sending and receiving ends is computed (see Fig. 5a).
2. By considering the voltage magnitudes (e_s and e_r) of the sending and receiving ends of the line, the angle necessary to have the flowing of a certain quantity of active power P_{sched} is (see Fig. 5b):

$$\vartheta_{sched} = \cos^{-1}\left(-\frac{B}{e_s e_r} p_{sched} + \frac{e_s D}{e_r}\cos(\beta - \delta)\right) - \beta \tag{10}$$

   which is the inverse formulation of (9). Therefore, ϑ_{sched} is the new shift angle between the two ends of the tie-line.
3. The swing angle displacement between the chosen areas can be computed as it follows (see Fig. 5b):

$$\vartheta'_{slack} = \vartheta_{sched} - \vartheta_{sr}. \tag{11}$$

   The interpretation of (11) is: ϑ'_{sched} is the shift angle missing to ϑ_{sr} to reach the scheduled value ϑ_{sched} by (10), between the two ends of the tie-line.
4. Finally, the swing bus of the receiving areas is shift by an angle equal to ϑ'_{slack}. Hence, if $\vartheta_{a,A}$=0, $\vartheta_{b,B} = -\vartheta'_{slack}$.
5. The basic procedure of Fig. 3 is computed again, by considering the angles of the involved swing generators as in point 4.

This modified version of the algorithm allows exploiting PFPD-X to discover the solution allowing the power flowing in a tie-lines to be near a scheduled value. A numerical application of the swing-correction PFPD-X is provided in Sect. V.

By means of the swing-correction PFPD-X, however, it is not possible to exactly constrain a scheduled active power flowing in a tie-line, in general. This is because the voltage magnitudes of the sending and receiving ends of the concerned tie-line change iteration by iteration (differently from the assumption adopted in (10)). However, this problem can be also found in the classical OPF algorithms, in which inequality constraints must be adopted in the concerned tie-lines [19].

The main drawback is that only the power flowing in few lines can be approached to a scheduled value. In a n-area power system, in fact, only $(n-1)$ tie-lines can be controlled by means of such method (one swing bus must be fixed as the reference, and the other $(n-1)$ swing bus can change). Even in this case, in the classical OPF algorithms it is not possible to fix an arbitrary number of constraints.

III. GENERALIZED THEVENIN'S THEOREM

Thevenin's theorem allows simplifying circuit computations by means of an equivalent representation seen from one port.

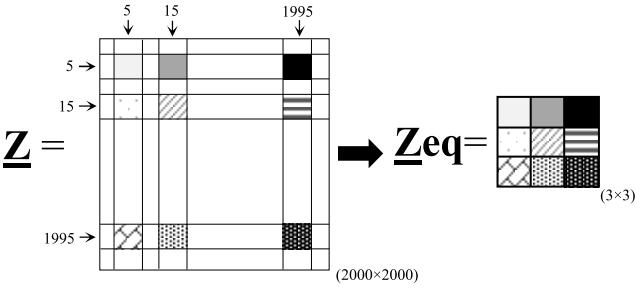

FIGURE 6. Example of impedance matrix reduction by means of the matrix extraction technique of a (2000 × 2000) "all-inclusive" impedance matrix.

In PFPD-X, a generalized Thevenin's equivalent representation is adopted: it is possible to study the steady-state network behavior as seen from n ports at the same time [20]. The generalization of the Thevenin's equivalent representation can be reached by means of tensor analysis. For this reason, as said in sect. I-A, it is advantageous to use PFPD inside PFPD-X [1], as an efficient matrix power flow computational tool.

This generalization is used to build the diagonal block matrix $\underline{\boldsymbol{Z}}_{\boldsymbol{eq}}$ in the second addend of (1), which computes the effect of the current injection on the voltages as seen from the cross-border nodes only. The blocks $\underline{\boldsymbol{Z}}_{\boldsymbol{Aeq}}$,$\underline{\boldsymbol{Z}}_{\boldsymbol{Beq}}$,$\underline{\boldsymbol{Z}}_{\boldsymbol{Ceq}}$ forming $\underline{\boldsymbol{Z}}_{\boldsymbol{eq}}$, are computed from the "all-inclusive" impedance matrices $\underline{\boldsymbol{Z}}_{\boldsymbol{A}}$,$\underline{\boldsymbol{Z}}_{\boldsymbol{B}}$,$\underline{\boldsymbol{Z}}_{\boldsymbol{C}}$ of each area.

The term "all-inclusive" refers to the fact that they are obtained by inversion of the "all-inclusive" admittance matrices $\underline{\boldsymbol{Y}}_{\boldsymbol{A}}$,$\underline{\boldsymbol{Y}}_{\boldsymbol{B}}$,$\underline{\boldsymbol{Y}}_{\boldsymbol{C}}$ of the areas [1], [14]. The expression "all-inclusive", in fact, means that both the network (nodes, AC lines, DC links, transformers, etc.) and power flow data (slack, PV, and PQ constraints) can be modelled and stored inside the nodal admittance matrix [1], [14].

Therefore, such matrices give a complete steady-state *snapshot* of the network. For the steps to compute the "all inclusive" admittance matrices, please see [1], [14].

Once the "all-inclusive" impedance matrices $\underline{\boldsymbol{Z}}_{\boldsymbol{A}}$, $\underline{\boldsymbol{Z}}_{\boldsymbol{B}}$, $\underline{\boldsymbol{Z}}_{\boldsymbol{C}}$ are computed, the equivalent matrices $\underline{\boldsymbol{Z}}_{\boldsymbol{Aeq}}$, $\underline{\boldsymbol{Z}}_{\boldsymbol{Beq}}$, $\underline{\boldsymbol{Z}}_{\boldsymbol{Ceq}}$ can be derived by means of the standard Gauss-Rutishauser model reduction technique [1], [14], [21], [22], [23]. Hence, $\underline{\boldsymbol{Z}}_{\boldsymbol{Aeq}}$, $\underline{\boldsymbol{Z}}_{\boldsymbol{Beq}}$, $\underline{\boldsymbol{Z}}_{\boldsymbol{Ceq}}$ represent the Ward equivalent networks as seen from the cross-border nodes [21]. The drawback of this procedure is the ease of mistake when the procedure is implemented. In fact, nodal-reorder procedures must be implemented to order the nodes in the correct entries.

A way to obtain the equivalent matrix can be derived by means of the impedance matrix extraction technique. Fig. 6 shows the (3 × 3) matrix extraction from a (2000 × 2000) impedance matrix $\underline{\boldsymbol{Z}}$ from the nodes 5, 15, and 1995. The reduced $\underline{\boldsymbol{Z}}_{\boldsymbol{eq}}$ impedance matrix describes the steady-state behavior of the network as seen from the cross-border nodes without any simplifying hypothesis. This reduction procedure gives benefits from a computational standpoint.

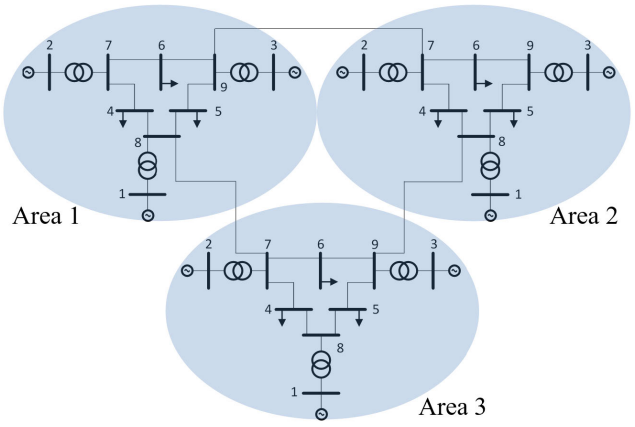

FIGURE 7. The 3-area interconnected power system test network (each area is the Anderson WSCC 3-machine).

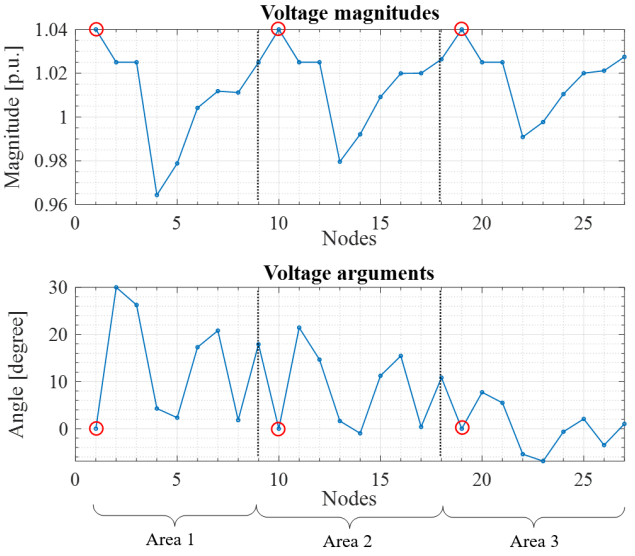

FIGURE 8. Overall voltage magnitudes and arguments for the 3-area power system. The red circles indicate the swing buses of each area, corresponding to nodes 1, 10, and 19. Like a power flow method, PFPD-X allows finding the voltage phasor of all the buses of a network under assessment.

IV. CASE STUDY I: THE BASIC PFPD-X PROCEDURE

To test PFPD-X, simulations on the 3-area power system of Fig. 7 is considered. The simulations consider the *basic* procedure. See Sect. V for simulation with the *swing-correction* procedure.

Each area of the 3-area power system is the WSCC 3-machine, 9-bus test system, developed by Anderson [24]. PFPD-X is implemented in Matlab environment. Please, see appendix A for the power flow data of the overall system.

All the simulations are performed by an Intel(R) Xeon(R) Gold 5222 CPU @ 3.80 GHz, RAM: 384 GB PC.

The convergence criterion is based on the evaluation of the cross-border voltage magnitude mismatches between two consecutive PFPD-X iterations k and $k-1$, *i.e.*,

$$\Delta e_k = e_k - e_{k-1} < tol$$

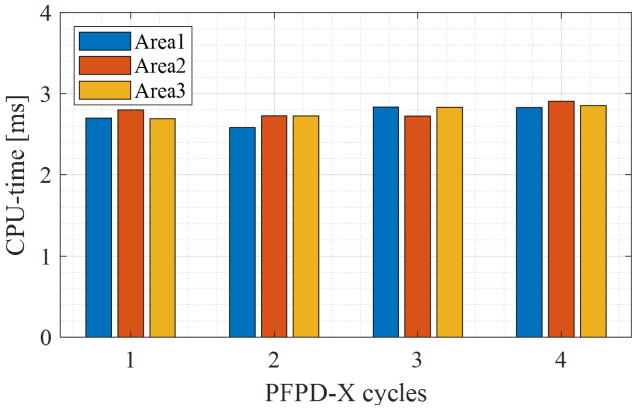

FIGURE 9. CPU-time trend for all the 3-area power flows executed in the overall cycle.

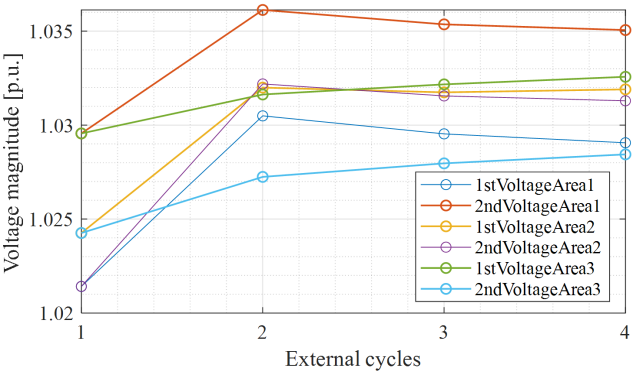

FIGURE 10. Convergence behavior of the cross-border voltage magnitudes of the 3-area power system of Fig. 7.

where *tol* is a chosen tolerance (typically set to the order of hundreds of volts in absolute values).

A. THE BASIC MULTIAREA ALGORITHM (SERIAL COMPUTING)

Fig. 8 shows the PFPD-X solution in terms of voltage phasor magnitudes and arguments of the 3-area power system. It can be noted that 1, 10, and 19 voltage arguments (the first nodes of each area, circled in red) are set to zero, since they represent the swing (and slack) generator buses for each of the three areas respectively.

The tolerance of PFPD-X was set to 10^{-3} p.u. (*i.e.*, in absolute values 230 V = 230 kV$\cdot$ 10^{-3} p.u.). It is worth citing that several tests show the convergence achievement of the algorithm even for PFPD-X relative voltage tolerance equal to 10^{-15} p.u.! Such low tolerances make no sense from a physical standpoint, but they demonstrate the very good convergence features of PFPD-X.

The simulation converges after 1.31 s in 4 iterations.

Fig. 9 is the bar plot representing the power flow CPU time of each power flow of each independent area. The mean CPU time of each area power flow computation is 0.0033 s.

Fig. 10 shows the convergence behavior of the six cross-border voltage magnitudes for each PFPD-X cycle. It is of note the convergence to a stable constant value. The active power generated by each slack generator are - 59.75 MW, -10.62 MW, and 112.59 MW respectively for area 1, 2, and 3. The active power flowing in tie-lines 1-2, 1-3, and 2-3 are 82.05 MW, -12.70 MW, and 23.40 MW respectively.

B. THE BASIC MULTIAREA ALGORITHM (PARALLEL COMPUTING)

As it is inferable from the flow chart of Fig. 3, power flow computations of the three areas can be run in parallel, by means of 3 workers. The simulations of Sect. IV-A are also performed by means of parallel computing at the same conditions. For the analyzed network, however, there are no significant CPU time reduction for the algorithm, since the number of nodes of the considered network is very low.

Notwithstanding, a dramatic CPU time decrease is to be expected with real transmission network simulations, with high number (1000+) of nodes.

C. VALIDATION OF PFPD-X

To validate PFPD-X, voltage comparisons with the commercial software DIgSILENT PowerFactory© (DGS) are performed. In the power flow problem, in fact, voltage magnitude and arguments are the minimum and sufficient set of solutions.

In DGS, it is not possible to perform a multi-area power flow: to make the comparisons, the same network is defined in both environments, and two PV nodes are defined in DGS where two arbitrary slack bus are defined in PFPD-X. Hence, only one slack generator in DGS can be defined.

After running the simulation in both environments, the maximum voltage phasor angle and magnitude mismatches are computed. The mismatches are 0.0014° for the voltage angles and 0.13% for the voltage magnitude.

D. A NUMERICAL APPLICATION: ACTIVE POWER CONTROL BY MEANS OF PFCs

In this sub-section, numerical applications show the capability of PFPD-X to make computations in presence of Power Flow Controllers (PFC). This choice is necessary since their importance in the management of active power in multi-area power systems.

PFCs are commonly used to control the electric power flows. Therefore, congestions, loop flows, and cross-border unscheduled power problems can be managed. However, PFCs must be coordinated in order not to worsen the overall system operation [25], [26].

By considering the 3-area system of Fig. 7, one PST for each tie-line is considered. PSTs are the transformers with quadrature voltage regulation and mechanical tap changers, currently present in power systems world. Fig. 11 schematizes the PST positioning and the conventions used to make

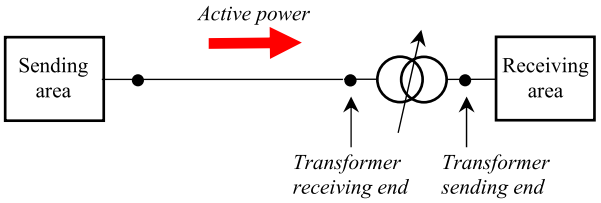

FIGURE 11. Conventions chosen for the areas and PSTs.

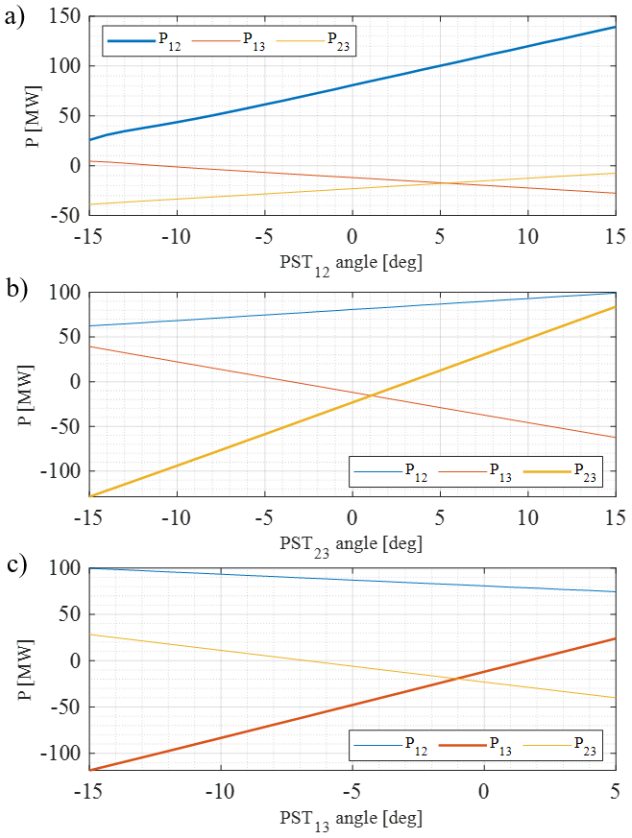

FIGURE 12. Active power flows in the three tie-lines by considering the angle changes a) of the PST_{12}, b) of the PST_{23}, c) of the PST_{13}.

the simulations. Fig. 12 shows the impact of the PST angle variation on the tie-line active power. The three characteristics a), b), and c) refer to the PSTs acting one by one. In particular, Fig. 12a) regards the impact on lines 1-2, 2-3, 1-3 in terms of active power, when the PST_{12} angle in line 1-2 is changed. Similarly, Fig. 12b), and 12c) refer to the impact of angle changes of PSTs in lines 2-3 and 1-3, respectively. It is worth noting the quasi-linear active power characteristic with respect to the angle [25]. The angle range chosen for the simulation is $[-15°, 15°]$, which is a typical angle variation for real-world installed PSTs. For the PST_{13}, it is shown the results for a range $[-15°, 5°]$, since in this case, power flow computational convergence is not guaranteed for angle settings greater than 5°. Tab. 1 reports the impacts in terms of active power changes in the tie-lines for each PST in action. It is worth observing that, also in the tie-lines in

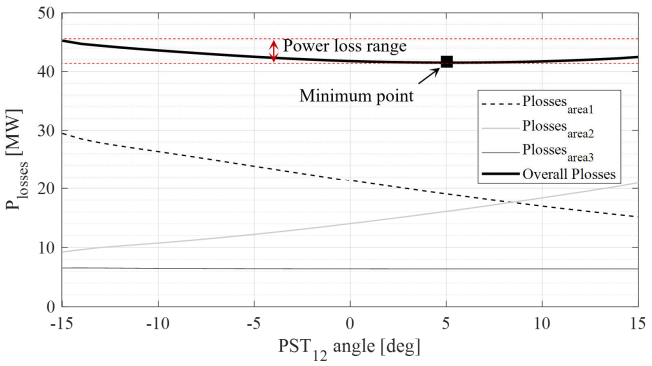

FIGURE 13. Impact of the PST_{12} angle (between areas 1 and 2) on the power losses.

TABLE 1. Tie-line power flow changes with the PST angle.

	MW/1°		
PST in action	Tie-line 12	Tie-line 13	Tie-line 23
PST_{12}	3.79	-1.07	1.046
PST_{13}	-1.26	7.13	-3.42
PST_{23}	1.22	-3.39	7.08

which the PST is not present, the active power changes are not negligible.

This fact confirms the need of a systemic/overall impact assessment whenever a PFC is going to be installed [25], [26]. In order to do this, different criteria can be adopted. One of the criteria adopted to assess the impact of a PST in the whole system and in each area can be the power loss evaluation. PFPD-X has the advantage of having a slack bus for each area, so giving the losses of its own area. The power losses P_{losses} of each area can be computed according to the following formulations:

$$P_{loss} = P_{slack} + \sum P_{PV} - \sum P_{PQ}$$

where P_{slack} is the active power solution injected by the slack generators; $\sum P_{PV}$ and $\sum P_{PQ}$ are the sum of the active power injected by the PV and PQ constraints respectively.

Therefore, impact in terms of power losses in neighboring systems and in the entire network can be assessed. For instance, Fig. 13 shows the power loss trend as a function of the PST_{12} angle. A minimum power loss value can be achieved for a PST_{12} angle equal to 5° (41.51 MW). However, a different behavior can be noted for each area (increasing function for area 2, decreasing one for area 3, and quasi-constant one for area 3).

Fig. 13 shows that the system power losses range from 41.51 MW to 45.27 MW, corresponding to a variation of 9.1% of the minimum active power value.

Moreover, Fig. 13 shows the quasi-constant behaviour of the power losses in area 3. The power losses of each area range from 29.49 MW to 15.17 MW for area 1 (losses decrease by 1.94 times), from 9.24 MW to 20.94 MW for area 2 (losses increase by 2.27 times), and from 6.55 MW to 6.37 MW for area 3 (the losses are quite the same varying by 2.82%). These loss values mean that, for this network, the PST_{12} has an impact only in the areas which connects.

TABLE 2. Active Power Comparison for the Tie-Lines connecting the three areas: the Standard and Swing-Corrected method are compared.

	Scheduled power	Standard method	Swing-corrected method
P_{12}	100 MW	82.01 MW	95.00 MW
P_{13}	50 MW	-12.71 MW	51.99MW
P_{23}	*Unconstrained*	-23.42 MW	-0.20MW

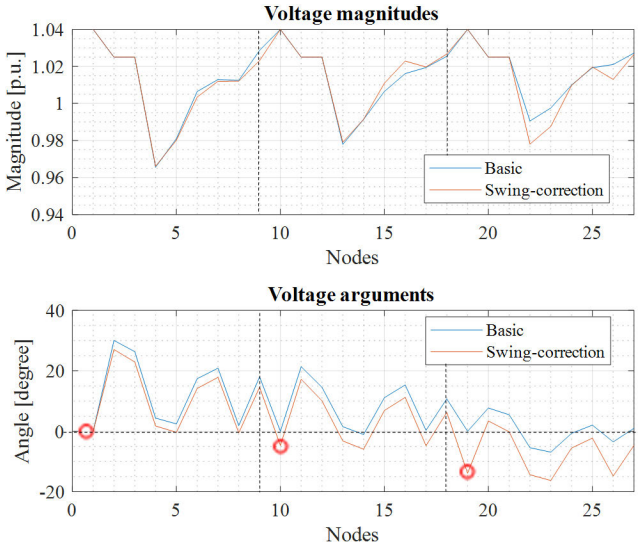

FIGURE 14. Solution comparison for the 3-areas power system adopting the basic and the swing correction-method. It is worth noting the overall variation on the voltage angles due to different transits of power.

V. CASE STUDY II: THE SWING-CORRECTION PFPD-X PROCEDURE

The method described in Sect. II-B is implemented to allow the transit of a power in 2 tie-lines near a constrained value. It is worth reminding that in a 3-area power system, 2 ($= n - 1$) tie-lines can be controlled, since the number of slack buses is 3 (n=3).

The active power generated by each slack generator are 16.59 MW, 1.98 MW, and 29.21 MW for area 1, 2, and 3, respectively. It is supposed to schedule the flow of active power in tie-lines 1-3 and 1-2. Table 2 reports the differences between the basic and the swing-correcting method for the transmitted power in the concerned tie-lines. With the swing-correcting method, active power difference of 5% and 3.98% for lines 1-2 and 1-3 respectively are found. For completeness, it is shown the computed active power flowing in the line 23 by using the two methods. This result shows that it is possible to control the flows on certain lines (no more than n-1 lines).

Fig. 14 shows the new results of the swing-correction technique in comparison with the basic technique for the

TABLE 3. Comparison of the Active Power Solution for the Tie-Lines connecting areas 1-2 and areas 1-3 of the Basic and Swing-Correction method (the loading is increased by +25%).

	Scheduled power	Standard method	Swing-corrected method
P_{12}	100 MW	106.34 MW	94.22 MW
P_{13}	50 MW	-16.82 MW	57.37 MW
P_{23}	*Unconstrained*	-29.15 MW	74.75 MW

TABLE 4. Active power given by the slack generators of the three areas.

	Bus 1	Bus 2	Bus 3
A	P_{Slack}=-59.8 MW	P_2=165 MW	P_3=140 MW
B	P_2=165 MW	P_{Slack}=-49.01 MW	P_3=140 MW
C	P_3=140 MW	P_2=165 MW	P_{Slack}=-45.2 MW

overall system. The corrected angles of the three slack buses of the three areas is highlighted by three red circles. It is worth noting that most of the differences are in the angle solutions. This means that even the possibility to act on modifying two active powers in two lines has an impact on all the angle solutions of the overall system.

To understand if the results of the active power control of the tie-lines is conditioned by the power flow data of the single areas, several tests were performed.

In particular, two groups of tests are performed. In the first typology, a variation on the input data (PV and PQ constraints) is done, and observations on the differences between the scheduled and the transit power are derived.

In the second one, the impact of the particular choice of slack bus on the solution is made.

A. ON THE CONTROLLABILITY OF TIE-LINE ACTIVE POWER

In the first test, a +25% increment of the loading in all the three areas is supposed (see appendix A for the data).

The results of Tab. 3 show that the swing-corrected method allows making the transit of active power nearer to the scheduled one (compare the first and third columns). Several other tests show that the method is not conditioned by the choice of the data.

Other techniques for solving the power flow problem keeping constrained the active power on the lines is the OPF for given power transfer constraints. The above-mentioned method, however, cannot be thought as a substitution of the OPF, it can be rather considered as an alternative method as long as the number of the tie-line to be controlled is $n-1$.

B. ON THE DEPENDENCE OF THE SLACK BUS CHOICE

In the second test group, the impact of different choices of the slack bus is assessed. In the following, three scenarios choosing the slack bus in the three generation nodes of the first area is analyzed (see Tab. 4). The results show that the solution is dependent on the position of the slack bus.

TABLE 5. Power flow data for the 27-BUS 3-Area power system represented in Fig. 7.

Overall buses	Single-area buses	Area	Type	P [MW]	Q [Mvar]	Vbase [kV]
1	1	1	Slack	-	-	16.5
2	2	1	PV	265	-	18.0
3	3	1	PV	260	-	13.8
4	4	1	PQ	125	50	230
5	5	1	PQ	150	30	230
6	6	1	PQ	100	35	230
7	7	1	PQ	0	0	230
8	8	1	PQ	0	0	380
9	9	1	PQ	0	0	380
10	1	2	Slack	-	-	16.5
11	2	2	PV	175	-	18.0
12	3	2	PV	120	-	13.8
13	4	2	PQ	125	50	230
14	5	2	PQ	150	30	230
15	6	2	PQ	100	35	230
16	7	2	PQ	0	0	230
17	8	2	PQ	0	0	380
18	9	2	PQ	0	0	380
19	1	3	Slack	-	-	16.5
20	2	3	PV	165	-	18.0
21	3	3	PV	140	-	13.8
22	4	3	PQ	125	50	230
23	5	3	PQ	150	30	230
24	6	3	PQ	100	35	230
25	7	3	PQ	0	0	230
26	8	3	PQ	0	0	380
27	9	3	PQ	0	0	380

VI. OPEN QUESTIONS

The present paper demonstrates the theoretical validity of a new matrix multi-area power flow solution, by means of numerical comparisons with DGS. This validation requires a simple and reference network. The authors intend to apply their algorithm to real multi-area networks by benefitting from parallel computing of many separate control area power flows. This would allow comparing the physical tie-line power flows with the commercial ones.

VII. CONCLUSION

The present open algorithm PFPD-X allows computing the power flow of multi-area networks by means of a multi-area power flow and not by means of a single-area approach. By means of PQ-constraint shunt admittances modeling the neighboring networks linked by tie-lines, PFPD-X firstly solves separately the power flows of each area (with its own slack-bus) and then compares the results by connecting the areas with the tie-lines modelled by their admittance matrix.

The possibility of having as many slack-generators as the number of areas allows each area to provide for its own power losses. This is not possible with a unique slack-bus for all the interconnected grids.

Once the convergence is reached, a comparison between the real physical flows (resulting from the computation) into the tie-lines and the commercial ones (resulting from a power flow scheduling in a given tie-line) can be performed: if

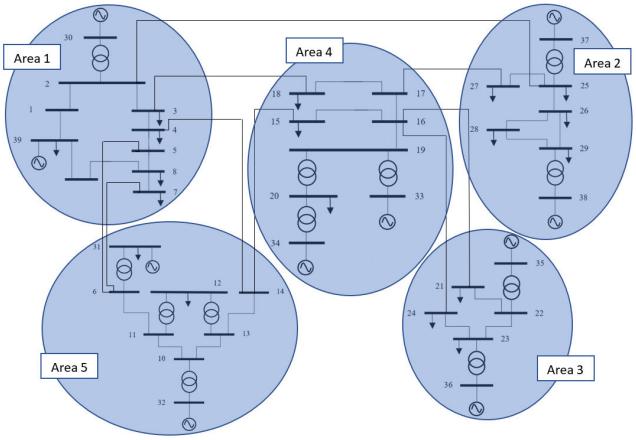

FIGURE 15. New England 39-bus standard network and identification of the five areas to be studied by means of PDPD_X.

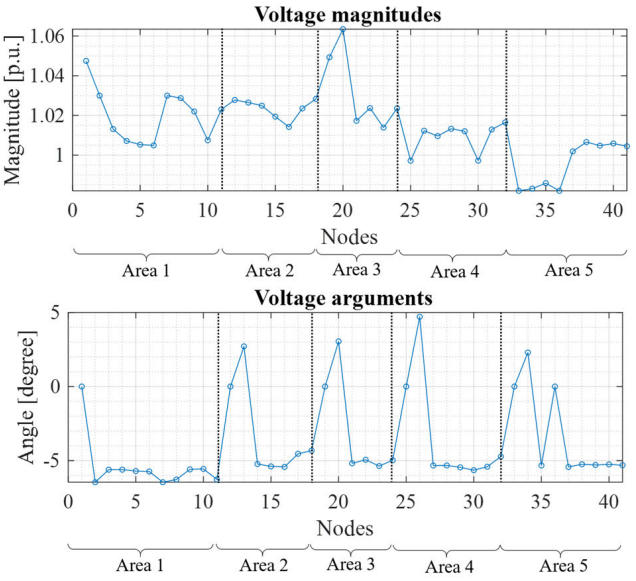

FIGURE 16. 39-bus standard network voltage magnitudes and arguments for the considered 5-area power system.

they are considerable different, it is possible to modify them on the basis of the slack-bus reference angles. Alternatively, it is possible to use PSTs in some tie-lines: in this case, the algorithm can compute the variation of the interconnection active power flows as a function of PST shifting angle.

APPENDIX A

The data of the three-area network of Fig. 7 are represented in Tab. 5.

APPENDIX B

The algorithm PFPD-X was tested on several multi-area power systems.

In this appendix, it is shown the application of PFPD-X on the 39-bus standard network (New England Test System).

TABLE 6. Number of iteration and CPU-time for four multi-area power systems with increasing number of nodes and areas.

	ITER	CPU time [s]
27-bus 3-area system	4	1.31
36-bus 4-area system	5	2.04
45-bus 5-area system	5	2.63
72-bus 8-area system	5	3.90

The system is subdivided into five areas represented in Fig. 15, each of which has its own slack generator.

Therefore, each of the five areas is considered as a separate grid, each one with the slack-generator providing its own power losses.

The multi-area power flow results of the overall network (see Fig. 16) are consistent with the ones of DGS, in accordance with what claimed in sect. IV-C.

APPENDIX C

In this appendix, a mention to the PFPD-X computational performances is presented, when the number of areas and nodes increases. The performances are presented in Tab. 6 in terms of number of iterations (ITER) and CPU time of PFPD-X.

It is worth reminding that the computational outcomes of PFPD-X are due to not-optimized self-made open access procedures. Authors think that optimized procedures made by software expert can dramatically decrease the computational times especially in terms of CPU-time.

REFERENCES

[1] R. Benato, "A basic AC power flow based on the bus admittance matrix incorporating loads and generators including slack bus," *IEEE Trans. Power Syst.*, vol. 37, no. 2, pp. 1363–1374, Mar. 2022.
[2] *Entso-e Official Website*. Accessed: Oct. 18, 2022. [Online]. Available: https://www.entsoe.eu/
[3] UCTE. (May 8, 2003). *Load-Flow Analysis With Respect to a Possible Synchronous Interconnection of Networks of UCTE and IPS/UPS*. [Online]. Available: https://eepublicdownloads.entsoe.eu/clean-documents/pre2015/publications/ce/otherreports/Load-Flow-study_UCTE_UPS_IPS-REPORT.pdf
[4] North American Electric Reliability Council. (Jun. 1992). *Control Area Concepts and Obligations*. [Online]. Available: https://web.archive.org/web/20110102152343/http://www.nerc.com/docs/docs/pubs/Control-Area-Concepts-and-Obligations.pdf
[5] R. Albert, I. Albert, and G. L. Nakarado, "Structural vulnerability of the North American power grid," *Phys. Rev. E, Stat. Phys. Plasmas Fluids Relat. Interdiscip. Top.*, vol. 69, no. 2, Feb. 2004, Art. no. 025103.
[6] N. Voropai, S. Podkovalnikov, and K. Osintsev, "From interconnections of local electric power systems to Global Energy Interconnection," *Global Energy Interconnection*, vol. 1, no. 1, pp. 4–10, 2018.
[7] S. Chatzivasileiadis, D. Ernst, and G. Andersson, "The global grid," *Renew. Energy*, vol. 57, pp. 372–383, Sep. 2013.
[8] M. Frick and M. Thioye, "Global electricity interconnection," *Global Energy Interconnection*, vol. 1, no. 4, pp. 404–405, Oct. 2018.
[9] G. Kron, "A set of principles to interconnect the solutions of physical systems," *J. Appl. Phys.*, vol. 24, no. 8, pp. 965–980, Aug. 1953.
[10] H. Kesavan, M. Pai, and M. Bhat, "Piecewise solution of the load-flow problem," *IEEE Trans. Power App. Syst.*, vol. PAS-91, no. 4, pp. 1382–1386, Jul. 1972.
[11] R. Andretich, D. Hansen, H. Brown, and H. Happ, "Pieccewise load fllow solutions of very large size networks," *IEEE Trans. Power App. Syst.*, vol. PAS-90, no. 3, pp. 950–961, May 1971.
[12] H. H. Happ, *Piecewise Methods and Applications to Power Systems*. New York, NJ, USA: Wiley, 1980.

[13] F. Wu, "Solution of large-scale networks by tearing," *IEEE Trans. Circuits Syst.*, vol. CAS-23, no. 12, pp. 706–713, Dec. 1976.
[14] R. Benato and G. Gardan, "A novel AC/DC power flow: HVDC-LCC/VSC inclusion into the PFPD bus admittance matrix," *IEEE Access*, vol. 10, pp. 38123–38136, 2022.
[15] X. Guoyu, F. D. Galiana, and S. Low, "Decoupled economic dispatch using the participation factors load flow," *IEEE Trans. Power App. Syst.*, vol. PAS-104, no. 6, pp. 1377–1384, Jun. 1985.
[16] A. Martinez-Mares and C. R. Fuerte-Esquivel, "A unified gas and power flow analysis in natural gas and electricity coupled networks," *IEEE Trans. Power Syst.*, vol. 27, no. 4, pp. 2156–2166, Nov. 2012.
[17] J. H. Chow and J. J. Sanchez-Gasca, "Steady-state power flow," in *Power System Modeling, Computation, and Control*. Hoboken, NJ, USA: Wiley, 2019, pp. 9–46.
[18] R. Benato and A. Paolucci, *EHV AC Undergrounding Electrical Power: Performance and Planning*. London, U.K.: Springer-Verlag, 2010.
[19] F. Milano, "Power flow devices," in *Power System Modelling and Scripting*. London, U.K.: Springer-Verlag, 2010.
[20] G. Corazza, C. Someda, and G. Longo, "Generalized Thevenin's theorem for linear N-port networks," *IEEE Trans. Circuit Theory*, vol. CT-16, no. 4, pp. 564–566, Nov. 1969.
[21] G. Kron, "Compound n-matrices," in *Tensors for Circuits*, 2nd ed. New York, NY, USA: Dover, 1959, pp. 14–20.
[22] R. Benato, G. Gardan, and L. Rusalen, "A three-phase power flow algorithm for transmission networks: A hybrid phase/sequence approach," *IEEE Access*, vol. 9, pp. 162633–162650, 2021.
[23] J. Grainger and W. Stevenson, *Power System Analysis*, 1st ed. New York, NY, USA: McGraw-Hill, 1994.
[24] P. M. Anderson and A. A. Fouad, *Power System Control and Stability*, 2nd ed. Piscataway, NJ, USA: IEEE Press, 2003.
[25] R. Korab and R. Owczarek, "Impact of phase shifting transformers on cross-border power flows in the central and eastern Europe region," *Bull. Polish Acad. Sci. Tech. Sci.*, vol. 64, no. 1, pp. 127–133, Mar. 2016.
[26] U. Häger, "Coordination methods for power flow controlling devices," in *Advanced Technologies for Future Transmission Grids*, G. Migliavacca, Ed. London, U.K.: Springer-Verlag, 2013, pp. 215–246.
[27] A. Pai, *Energy Function Analysis for Power System Stability*. New York, NY, USA: Springer, 1989.
[28] T. Athay, R. Podmore, and S. Virmani, "A practical method for the direct analysis of transient stability," *IEEE Trans. Power App. Syst.*, vol. PAS-98, no. 2, pp. 573–584, Mar. 1979.

ROBERTO BENATO (Senior Member, IEEE) was born in Venezia, Italy, in 1970. He received the Dr. (Ing.) degree in electrical engineering from the University of Padova, in 1995, and the Ph.D. degree in power systems analysis, in 1999. In 2021, he was appointed as a Full Professor with the Department of Industrial Engineering from Padova University, Padova, Italy. He is the author of 200 papers and five books, edited by Springer, Wolters Kluwer, Amazon KDP, and China Machine Press. He has been a member of the Six Cigré Working Groups (WGs), a Secretary of Two Joint WGs, and a member of IEEE PES Substations Committee. In 2014, he was nominated as a member of the IEC TC 120 "Electrical Energy Storage (EES) Systems" in the WG 4 "Environmental Issues of EES Systems." Currently, he is also a corresponding member of Cigré WG B1.72 "Cable Rating Verification Second Part." In 2018, he was elevated to the grade of a CIGRÉ distinguished member. He is a member of Italian AEIT.

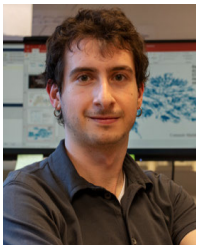

GIOVANNI GARDAN (Member, IEEE) was born in Venezia, Italy, in 1995. He received the B.S. degree in energy engineering and the Dr. (Ing.) degree in electrical engineering from the University of Padova, in 2017 and 2020, respectively. He is currently pursuing the Ph.D. degree in industrial engineering. His research interests include electrical energy transmission and power systems computation. He is a young member of Cigrè and AEIT.

Open Access funding provided by 'Università degli Studi di Padova' within the CRUI CARE Agreement